Irradiation-Induced Formation of Nanocrystallites with *C*15 Laves Phase Structure in bcc Iron

M.-C. Marinica, F. Willaime,* and J.-P. Crocombette

CEA, DEN, Service de Recherches de Métallurgie Physique, F-91191 Gif-sur-Yvette, France

(Received 28 September 2011; revised manuscript received 22 November 2011; published 11 January 2012)

A three-dimensional periodic structure is proposed for self-interstitial clusters in body-centered-cubic metals, as opposed to the conventional two-dimensional loop morphology. The underlying crystal structure corresponds to the *C*15 Laves phase. Using density functional theory and interatomic potential calculations, we demonstrate that in α-iron these *C*15 aggregates are highly stable and immobile and that they exhibit large antiferromagnetic moments. They form directly in displacement cascades, and they can grow by capturing self-interstitials. They thus constitute an important new element to account for when predicting the microstructural evolution of iron base materials under irradiation.

DOI: 10.1103/PhysRevLett.108.025501 PACS numbers: 61.72.Bb, 61.72.jj, 61.80.Az, 61.82.Bg

Point defect supersaturation occurs in crystals after quench from a high temperature, during mechanical deformation, or after irradiation by high energy particles [1]. By thermal migration, these defects can annihilate at sinks (surfaces, grain boundaries, and dislocations), recombine with their antidefects, or cluster with other defects [2,3]. Molecular dynamics (MD) simulations indicate that for irradiation by ions or neutrons a significant fraction of the defect population created in cascades is produced already in clusters [4,5]. The morphology adopted by these defect clusters is a fundamental question with obvious practical consequences on the materials properties, since it controls (i) the cluster mobility and hence the kinetics of the microstructure [6], (ii) the dislocation-obstacle strength [7,8] and hence the hardening of the materials, and (iii) dimensional changes like swelling or growth [3].

The morphology of vacancy clusters is fairly well known and quite diverse. There is a competition between planar loops and voids, both being experimentally evidenced [9,10]. In face-centered-cubic (fcc) metals and alloys, vacancy clusters also often form stacking fault tetrahedra having 3D pyramidal structure [11,12]. On the other hand, the observation of clusters of self-interstitial atoms (SIAs) in metals by transmission electron microscopy (TEM) techniques reveals only nanometer-size planar loops [9,13]. In body-centered-cubic (bcc) metals, these loops have a $1/2\langle 111\rangle$ Burgers vector, except in iron at high temperatures where it is $\langle 100\rangle$ [14,15]. SIA clusters formed in MD simulations of cascades contain only at most a few tens of SIAs, and they most often exhibit a morphology akin to dislocation loops. However, Bacon *et al.* observed that in iron 30%–50% of the clustered population of SIAs have a different morphology that renders them immobile, in contrast to the highly mobile ''glissile'' loops [5,16]. Quantitative insight into low energy structures of small SIA clusters in iron was gained from density functional theory (DFT) calculations. In agreement with experiments [17], the single SIA is the $\langle 110\rangle$ dumbbell [18,19]. This is a specificity of Fe, since in other bcc transition metals the defect is aligned in, or close to, the $\langle 111\rangle$ direction, forming a crowdion [20]. Dumbbells can be packed together in bundles, forming small dislocation loops. DFT predicts that in Fe the orientation of these dumbbells changes from $\langle 110\rangle$ to $\langle 111\rangle$ above around five SIAs [21]. However, other configurations have slightly lower energies according to DFT: for the di-interstitial, a triangular configuration with three atoms sharing the same site, and for the tri-interstitial a hexagonal ring configuration consisting of three nonparallel $\langle 110\rangle$ dumbbells [22]. In this Letter, we show that the 3D morphology observed for some ''sessile'' clusters in cascade simulations [5,16] corresponds to a particular metastable crystal structure, namely, that of the *C*15 Laves phase, and that in α-Fe these clusters have by far the lowest energy for four SIAs or more according to DFT calculations. Their mobility and their nucleation and growth mechanisms are investigated.

The starting point of the proposed new family of SIA clusters is the cagelike di-interstitial represented in Fig. 1(a). In terms of SIAs and vacancies, this defect corresponds to 12 SIAs, placed at the edges of a truncated tetrahedron, surrounded by 10 vacancies, which makes a total of only two additional atoms in the bcc lattice. One can recognize that the symmetric structure formed around the central atom by its $12 + 4$ nearest neighbors corresponds to the *Z*16 Frank-Kasper polyhedron [23]. Another *Z*16 polyhedron with 6 neighbors in common can then be constructed by adding 6 SIAs and 4 vacancies. This makes a tetra-interstitial, I_4 [Fig. 1(c)]. The two polyhedra have different orientations, and they are centered on two nearest neighbors of the bcc lattice. Other polyhedra can be added, forming clusters with 6 and 8 SIAs as illustrated in Figs. 1(d) and 1(e). By repeating this process, 3D clusters having a cubic periodic structure can be built. This crystallographic structure corresponds to the *C*15 Laves phase, or $MgCu_2$ structure [Fig. 1(f)] [24]. In this homoatomic type of *C*15 structure, interstitials occupy the Cu sites and half of the original bcc sites are empty while the others are occupied and correspond to the Mg

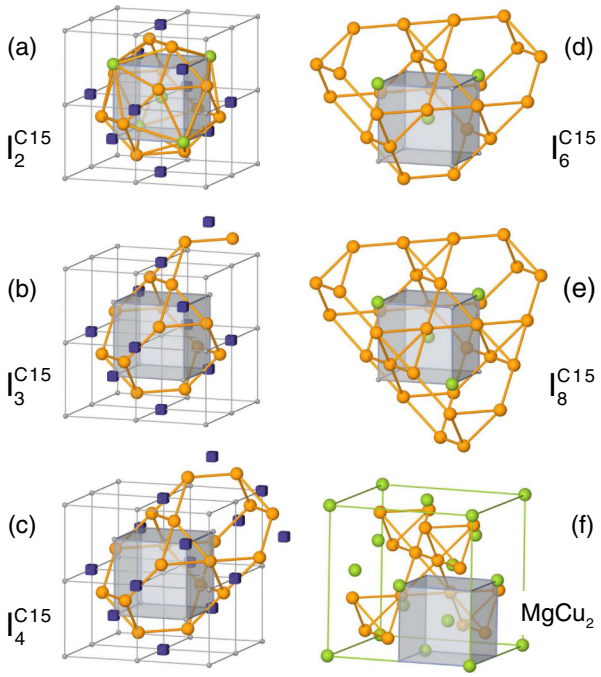

FIG. 1 (color online). Structure of small $C15$ interstitial clusters in the bcc lattice. (a)–(c) Representation by vacancies (blue cubes) and interstitials (orange spheres) of the di-, tri-, and tetra-interstitial clusters. For the di-interstitial, the atoms of the bcc lattice at the center and at the edges of the $Z16$ Frank-Kasper polyhedron are also represented (green spheres). (d),(e) Skeleton representation, i.e., without the vacancies and the cubic lattice and with the atoms at the center of the $Z16$ polyhedra in green, of the hexa- and octa-interstitials. (f) Unit cell of the $MgCu_2$ $C15$ Laves structure, with the Mg atoms in green and the Cu atoms in orange. For every cluster with 3 SIAs or more, the variant with the lowest energy found within DFT in Fe is represented.

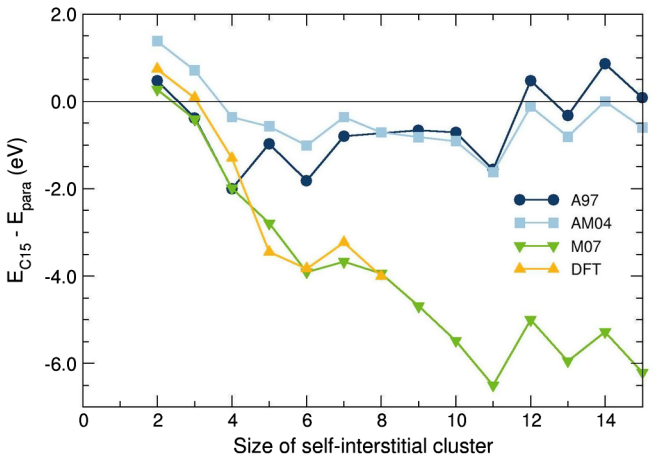

FIG. 2 (color online). Formation energies of the $C15$ SIA clusters in bcc Fe calculated with respect to the lowest energy parallel-dumbbell configurations, i.e., with a $\langle 110 \rangle$ orientation up to 4 SIAs and a $\langle 111 \rangle$ orientation at larger sizes. The DFT results are compared to those of three empirical potentials A97 [33], AM04 [34], and M07 [32].

sites. These SIA clusters will hereafter be denoted I_n^{C15}, where n is the net number of SIAs, i.e., the number of additional atoms in the bcc lattice.

The formation energy of these $C15$ SIA clusters, relative to that of other known forms of SIA clusters, was investigated in all bcc transition metals by performing DFT calculations using the PWSCF code [25]. We employed the ultrasoft pseudopotential scheme including semicore states for all metals except Fe, the Perdew-Burke-Ernzerhof generalized gradient approximation exchange correlation functional, and a 30 Ry plane wave energy cutoff. The calculations in Fe are spin polarized. We used a supercell with $250 + n$ atoms, where n is the number of SIAs, a $3 \times 3 \times 3$ k-point grid, and a 0.3 eV Hermite Gaussian broadening. The cell volume was rescaled proportional to the number of atoms. The remarkable result is that in iron the I_4^{C15}, I_6^{C15}, and I_8^{C15} clusters are found to have much lower energies than the most stable clusters formed by parallel dumbbells, respectively, by -1.3, -3.83, and -4.0 eV as shown in Fig. 2. This exceptional stability was confirmed by repeating the calculations for tetra-interstitials using either the projector augmented wave method and/or including semicore states. It is also confirmed and even enhanced within local-density approximation. The I_2^{C15} cluster is higher in energy than the parallel dumbbells by 0.74 eV and than the triangle by 0.85 eV, but it is still more stable than two isolated $\langle 110 \rangle$ dumbbells by 0.09 eV.

A number of binary and ternary alloys are known to crystallize in the $C15$ compact structure, but pure metals have never been observed in this structure [26]. In the present DFT calculations, we find that in Fe, bulk $C15$ in the ferromagnetic state is only 0.14 eV per atom higher in energy than the bcc ferromagnetic ground state. This excess energy is comparable to that of the metastable fcc structure that is observed, for instance, when thin layers of Fe are grown on fcc metals like Cu, Pd, or Pt. The $C15$ SIA clusters can be seen as coherent "homoprecipitates" of metastable $C15$ Fe, locally stabilized by the surrounding bcc Fe matrix. According to DFT calculations, in V, Nb, Ta, Cr, Mo, and W the bulk $C15$ structure also has a low energy, in particular, in group VB metals, but the I_4^{C15} cluster is always significantly higher in energy than the configuration made by four parallel $\langle 111 \rangle$ crowdions [27]. The energy difference is typically 2–3 eV, except in Ta where it is only 0.8 eV (see Table I). This atypical behavior of Fe with respect to the other bcc transition metals confirms the uniqueness of Fe regarding SIA properties [20]. The particular stability of the $C15$ SIA clusters in Fe can be related to the fact that they are assemblies of two types of building blocks that have low energies in Fe: the triangular di-interstitial and the hexagonal ring tri-interstitial [22]. A striking feature, that may contribute explaining the specificity of Fe, is the important changes in local magnetic moments in the $C15$ SIA clusters with a total antiferromagnetic moment with respect to the bulk supercell for

TABLE I. DFT results for the properties related to the $C15$ Laves phase in bcc transition metals: relative stability between the bcc and $C15$ structures, $\Delta E_b = E_{C15} - E_{\mathrm{BCC}}$ in eV/atom, and formation energy difference between the $\langle 111 \rangle$ and $C15$ morphologies of tetra-interstitials, $\Delta E_f = E_f(I_4^{C15}) - E_f(I_4^{\langle 111 \rangle})$ in eV.

	V	Nb	Ta	Cr	Mo	W	Fe
ΔE_b	0.113	0.159	0.112	0.277	0.372	0.453	0.142
ΔE_f	3.07	2.23	0.79	2.40	3.22	1.87	−3.14

I_4^{C15}, I_6^{C15}, and I_8^{C15} of, respectively, -33, -72, and $-96\mu_B$. This strong decrease in magnetic moment is confirmed and even enhanced within the local-density approximation according to calculations performed for I_4^{C15}. In the present generalized gradient approximation calculations, the interstitial atoms have a $-0.7\mu_B$ antiferromagnetic moment, compared to $+2.3\mu_B$ for bulk bcc atoms. The modulus of the magnetic moments of the surrounding atoms is also reduced to $1.9\mu_B$ [28]. The energy is always found to be lower when the atoms at the center of the $Z16$ cages are ferromagnetic with respect to the bcc matrix, except for I_2^{C15} (and I_3^{C15}; see below) where it is antiferromagnetic, with a magnetic moment as low as $-2.4\mu_B$ [28].

The unprecedented stability of I_4^{C15}, I_6^{C15}, and I_8^{C15} within DFT in bcc Fe makes the $C15$ configurations very good candidates for the lowest energy structures of small SIA clusters. Further evidence is brought by a systematic exploration of the energy landscape of SIA clusters, using the activation relaxation technique nouveau (ARTn) [29–31] and an embedded-atom method potential for Fe, denoted M07 [32]. This potential was fitted to a large database of DFT defect formation energies, and it was chosen here because it reproduces very well the DFT features of $C15$ interstitial clusters, at variance with other reference potentials for Fe [33,34], as illustrated in Fig. 2. The low energy part of the energy landscape obtained for the tetra-interstitial from the 10^6 lowest energy minima found by ARTn is represented in Fig. 3(a) by using the disconnectivity graph method [35–37]. The $C15$ structure is confirmed to be by far the lowest energy structure, i.e., by more than 1.5 eV. The lowest energy barrier to escape from this deep minimum is 1.9 eV. Moreover, no low energy direct path between two adjacent positions of $C15$ clusters was found. It follows that the I_4^{C15} cluster is expected to be highly immobile. MD simulations performed at 300–600 K confirm that the I_4^{C15} aggregate does not migrate at all over times as large as 1 μs. In the lower part of the disconnectivity graph, two distinct superbasins are observed. They correspond, respectively, to the parallel dumbbells and $C15$ structures [see Fig. 3(a)]. When the system is quenched from high energy and/or high temperature, e.g., in a cascade, it can fall into one of these two superbasins, but once it is in the parallel-dumbbell configuration, the energy barrier to transform to the $C15$ structure is 0.94 eV. This transformation is therefore highly infrequent, except at very high temperatures, and this suggests that the two types of morphologies should coexist.

One may wonder whether these highly stable and immobile defect clusters can actually form under or after irradiation and whether they can grow by capturing other SIA defects. These two questions have been addressed by

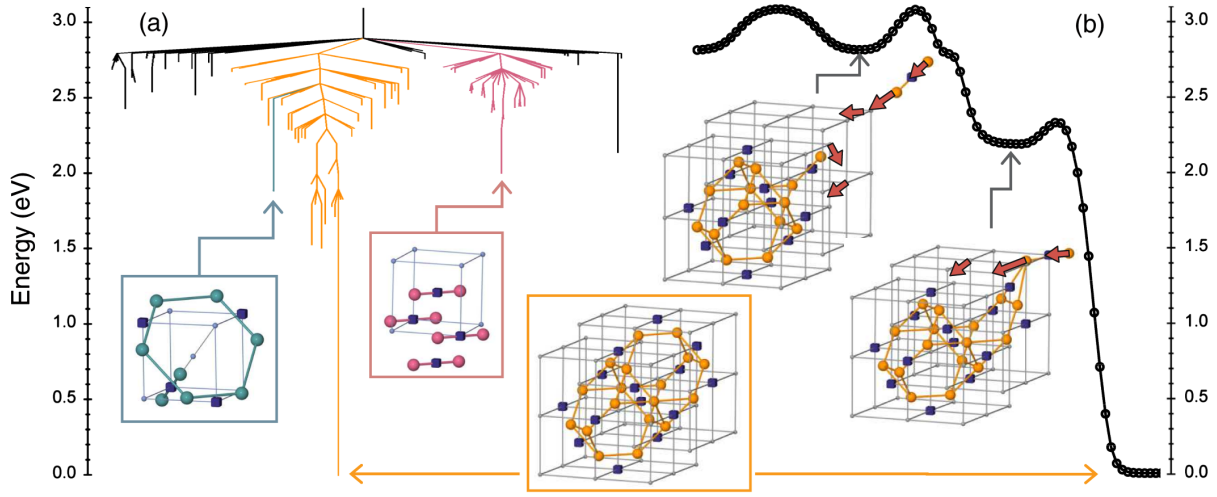

FIG. 3 (color online). Energy landscape of tetra-interstitial clusters obtained by using the ARTn method and the M07 potential for Fe. (a) Disconnectivity graph representation; the main superbasins include the structures related, respectively, to the parallel-dumbbell configuration (in pink) and the $C15$ configuration (in orange); the ring configuration as part of the $C15$ basin is shown in blue. (b) Growth mechanism of $C15$ interstitial clusters in iron illustrated by the formation of a I_4^{C15} cluster from the capture of a migrating $\langle 110 \rangle$ dumbbell by a I_3^{C15}; the reaction pathway between local minima was determined by using the nudged elastic band method. The arrows indicate the displacements of atoms for the transformation to the next local minimum configuration.

using MD, ARTn, and the M07 potential. To mimic the primary state of damage under ion or neutron irradiation, we have performed a series of 100 cascade simulations with a kinetic energy of 20 keV for the primary knock-on atom and various initial orientations at temperatures ranging from 300 to 900 K [38]. About half of the SIAs are clustered. Analyzing the structure of these clusters, we found that about 5% of them are of the $C15$ type, either perfect or with some defects in it. The I_2^{C15} di-interstitial is sometimes formed, but most of the observed $C15$-type clusters are larger, with up to 12 SIAs. In these clusters $\langle 110 \rangle$ dumbbells, triangular, or hexagonal ring units are frequently attached to $Z16$ polyhedra. These results are consistent with previous cascade simulations performed with a different interatomic potential, where a structure corresponding to the I_2^{C15} cluster was observed [5] as well as larger clusters that can be identified to have a $C15$ structure [16].

Once formed during cascades, though in small amount, these clusters can grow by capturing mobile SIA defects. We indeed identified low energy pathways for the formation of I_{n+1}^{C15} from the reaction between I_n^{C15} clusters and mobile $\langle 110 \rangle$ dumbbells. So far, we have described only closed shell structures, like that of I_2^{C15}, I_4^{C15}, and I_6^{C15} displayed in Fig. 1, i.e., structures formed only by perfect $Z16$ polyhedra. At small sizes, i.e., up to $n = 10$, these clusters contain an even number of SIAs, but this is not a general rule, since, for instance, I_{11}^{C15} is also a closed shell structure for geometrical reasons. Low energy structures can also be formed by attaching a $\langle 110 \rangle$ dumbbell to these clusters. For instance, the lowest energy structure found by ARTn for the tri-interstitial with the M07 potential is a I_2^{C15} cluster with a $\langle 110 \rangle$ dumbbell attached to it [see Fig. 1(b)]. No lower energy structure was found within DFT (see Fig. 2). The situation is similar for I_5^{C15}, I_7^{C15}, and I_9^{C15} as well as for I_{12}^{C15}. We will therefore describe two types or reactions: the formation of a $C15$ structure with a dangling $\langle 110 \rangle$ dumbbell starting from a perfect closed shell structure and an isolated $\langle 110 \rangle$ dumbbell and the formation of a closed shell structure. The first type of reaction is rather straightforward, and we have indeed checked, in the case of the reaction $I_2^{C15} + I^{\langle 110 \rangle} \rightarrow I_3^{C15}$, that there is at least one reaction pathway with an activation barrier not higher than that of the migration of the free $\langle 110 \rangle$ dumbbell, i.e., 0.3 eV. By analyzing the results of the ARTn simulation, a more complex but also low energy reaction pathway could be found for the reaction $I_3^{C15} + I^{\langle 110 \rangle} \rightarrow I_4^{C15}$ as an illustration of the second type of reaction. It can be seen in Fig. 3(b) that again no barrier is higher than the first one that corresponds to the free migration of the $\langle 110 \rangle$ dumbbell. Similar reaction pathways are expected for larger clusters for both types of reactions.

According to the empirical potential calculations, the formation energy of I_n^{C15} clusters relative to that of $\langle 111 \rangle$ loops continues decreasing until $n = 11$; it is then approximately the same until about $n = 15$ (see Fig. 2). Further investigations are required to see how further growth is altered by other effects like strain or bcc-$C15$ interface lattice mismatch. At large sizes the loop morphology is expected to have a lower energy, but once the cluster starts growing in the three-dimensional $C15$ morphology, it cannot easily convert into the two-dimensional loop shape.

In the absence of cascades, e.g., under electron irradiation, the nucleation process of these $C15$ SIA clusters is less clear. From our ARTn simulations a direct transformation to $C15$ from either the triangular di-interstitial or the parallel-dumbbell tetra-interstitial can be excluded, since the activation barriers are as high as 1.5 and 1 eV, respectively.

We have presented computer simulation evidence for the existence of three-dimensional SIA clusters with $C15$-type structure in bcc Fe. These clusters are predicted to have very low formation energies and to be highly immobile. They are shown to form in cascades. While they amount only to a few percent of the total number of SIA clusters produced in the primary state of damage, these clusters can grow by capturing mobile $\langle 110 \rangle$ dumbbells. Moreover, they will not annihilate at sinks as they cannot migrate. They are still likely to represent only a small fraction of the defect clusters and this may explain why they have not been identified in TEM observations so far. Their large antiferromagnetic moments may also provide a way to detect them [39]. Despite their low concentration, these clusters are expected to play a crucial role in the behavior of iron and ferritic steels under irradiation. These clusters may indeed first contribute to the hardening tendency observed in iron at low irradiation doses [40]. They are also very good candidates for the fraction of the SIA clusters that need to be assumed to be immobile in kinetic simulations of defect evolution in order to account for experimental observations [6]. Irradiation-induced phase transformations, i.e., transformations that drive the system to a state that is distinct from its thermal equilibrium configuration, are a well known phenomenon in alloys and compounds [41]. The transformation of graphite to diamond is an example in pure systems [42]. The formation of $C15$ nanocrystallites proposed here can be seen as a local irradiation-induced phase transformation from bcc to $C15$ in pure iron. Similarly, refractory metals were shown to form a metastable $A15$ phase when solidified from undercooled liquids, i.e., under other nonequilibrium conditions [43].

The authors thank F. Ducastelle for identifying the $MgCu_2$ Laves phase structure and M. Fluss, D. Rodney, and B. Legrand for suggestions and critical reading of the manuscript. M.-C. M. acknowledges insightful discussions with D. J. Wales on disconnectivity graphs. This work was carried out in the frame of the Perform60 project from the European Community's Seventh Framework Program under Grant No. 232612. The calculations were performed by using HPC resources from the CINES computer center.

*francois.willaime@cea.fr

[1] R. S. Averback and T. Diaz de la Rubia, in *Displacement Damage in Irradiated Metals and Semiconductors*, edited by H. Ehrenfest and F. Spaepen, Solid State Physics Vol. 51 (Academic, New York, 1997).

[2] X.-M. Bai, A. F. Voter, R. G. Hoagland, M. Nastasi, and B. P. Uberuaga, Science **327**, 1631 (2010).

[3] G. S. Was, *Fundamentals of Radiation Materials Science* (Springer-Verlag, Berlin, 2007).

[4] R. E. Stoller, G. R. Odette, and B. D. Wirth, J. Nucl. Mater. **251**, 49 (1997).

[5] D. J. Bacon, F. Gao, and Y. Osetsky, J. Nucl. Mater. **276**, 1 (2000).

[6] C.-C. Fu, J. Dalla Torre, F. Willaime, J.-L. Bocquet, and A. Barbu, Nature Mater. **4**, 68 (2005).

[7] D. Rodney and G. Martin, Phys. Rev. Lett. **82**, 3272 (1999).

[8] T.Diaz de la Rubia, H. M. Zbib, T. A. Khraishi, B. D. Wirth, M. Victoria, and M. J. Caturla, Nature (London) **406**, 871 (2000).

[9] M. L. Jenkins and M. A. Kirk, *Characterization of Radiation Damage by Transmission Electron Microscopy* (Institute of Physics, Bristol, 2001).

[10] Y. Matsukawa and S. J. Zinkle, Science **318**, 959 (2007).

[11] J. Silcox and P. B. Hirsch, Philos. Mag. **4**, 72 (1959).

[12] K. Nordlund and F. Gao, Appl. Phys. Lett. **74**, 2720 (1999).

[13] K. Arakawa, K. Ono, M. Isshiki, K. Mimura, M. Uchikoshi, and H. Mori, Science **318**, 956 (2007).

[14] B. C. Masters, Nature (London) **200**, 254 (1963).

[15] S. L. Dudarev, R. Bullough, and P. M. Derlet, Phys. Rev. Lett. **100**, 135503 (2008).

[16] F. Gao, D. J. Bacon, Y. N. Osetsky, P. E. J. Flewitt, and T. A. Lewis, J. Nucl. Mater. **276**, 213 (2000).

[17] P. Ehrhart, K. H. Robrock, and H. R. Schober, in *Physics of Radiation Effects in Crystals*, edited by R. A. Johnson and A. N. Orlov (Elsevier, Amsterdam, 1986), p. 63.

[18] C. Domain and C. S. Becquart, Phys. Rev. B **65**, 024103 (2001).

[19] C.-C. Fu, F. Willaime, and P. Ordejon, Phys. Rev. Lett. **92**, 175503 (2004).

[20] D. Nguyen-Manh, A. P. Horsfield, and S. L. Dudarev, Phys. Rev. B **73**, 020101 (2006).

[21] F. Willaime, C.-C. Fu, M.-C. Marinica, and J. Dalla Torre, Nucl. Instrum. Methods Phys. Res., Sect. B **228**, 92 (2005).

[22] D. A. Terentyev, T. P. C. Klaver, P. Olsson, M.-C. Marinica, F. Willaime, C. Domain, and L. Malerba, Phys. Rev. Lett. **100**, 145503 (2008).

[23] F. C. Frank and J. S. Kasper, Acta Crystallogr. **11**, 184 (1958).

[24] F. Laves and H. Witte, Metallwirt. **14**, 645 (1935).

[25] P. Giannozzi *et al.*, J. Phys. Condens. Matter **21**, 395502 (2009).

[26] F. Ducastelle, *Order and Phase Stability in Alloys* (Elsevier Science, New York, 1991).

[27] Because of the complexity of its magnetic structure, Cr was treated in the paramagnetic approximation.

[28] See Supplemental Material at http://link.aps.org/supplemental/10.1103/PhysRevLett.108.025501 for the illustration of the magnetic moments in the I_2^{C15} and I_4^{C15} structures.

[29] G. T. Barkema and N. Mousseau, Phys. Rev. Lett. **77**, 4358 (1996).

[30] R. Malek and N. Mousseau, Phys. Rev. E **62**, 7723 (2000).

[31] M.-C. Marinica, F. Willaime, and N. Mousseau, Phys. Rev. B **83**, 094119 (2011).

[32] The fitting procedure, parameters, and defect properties of the M07 potential developed by M.-C. Marinica in 2007 are described in L. Malerba *et al.*, J. Nucl. Mater. **406**, 19 (2010); note that the correct value for the B_1 parameter is with a negative sign.

[33] G. J. Ackland, D. J. Bacon, A. F. Calder, and T. Harry, Philos. Mag. A **75**, 713 (1997).

[34] G. J. Ackland, M. I. Mendelev, D. J. Srolovitz, S. Han, and A. V. Barashev, J. Phys. Condens. Matter **16**, S2629 (2004).

[35] O. M. Becker and M. Karplus, J. Chem. Phys. **106**, 1495 (1997).

[36] D. J. Wales, M. A. Miller, and T. Walsh, Nature (London) **394**, 758 (1998).

[37] The disconnectivity graphs were created by using the disconnection DPS code developed by M. Miller, D. J. Wales, and V. de Souza in the OPTIM package, http://www-wales.ch.cam.ac.uk/software.html.

[38] J. P. Crocombette, in *Handbook of Materials Modeling*, edited by S. Yip (Springer, Berlin, 2005), p. 987.

[39] S. K. McCall, M. J. Fluss, B. W. Chung, M. W. McElfresh, D. D. Jackson, and G. F. Chapline, Proc. Natl. Acad. Sci. U.S.A. **103**, 17 179 (2006).

[40] S. J. Zinkle and B. N. Singh, J. Nucl. Mater. **351**, 269 (2006).

[41] G. Martin and P. Bellon, C.R. Physique **9**, 323 (2008).

[42] M. Zaiser and F. Banhart, Phys. Rev. Lett. **79**, 3680 (1997).

[43] L. Cortella *et al.*, Phys. Rev. Lett. **70**, 1469 (1993).